2

Simulations of Deformation Processes in Energetic Materials

R.H.B. Bouma[1], A.E.D.M. van der Heijden[1],
T.D. Sewell[2] and D.L. Thompson[2]
[1]*TNO Technical Sciences*
[2]*University of Missouri*
[1]*The Netherlands*
[2]*USA*

1. Introduction

The sensitivity of energetic materials has been studied extensively for more than half a century, both experimentally and numerically, due to its importance for reliable functioning of a munition and avoidance or mitigation of accidents (Bowden & Yoffe, 1952). While the shock initiation of an explosive under nominal conditions is relatively well understood from an engineering perspective, our understanding of initiation due to unintended stimuli (weak shock or fragment impact, fire, damaged explosive charge) is far less complete. As an example, one cannot exclude the ignition of an explosive due to mechanical deformation, potentially leading to low- or even high-order explosion/detonation as a consequence of mechanical stimuli with strain rates and pressures well below the shock sensitivity threshold. During the last two decades there has been an increased interest in the scientific community in understanding initiation sensitivity of energetic materials to weak insults.

A relationship between energy dissipation and rate of plastic deformation has been developed for crystalline energetic materials (Coffey & Sharma, 1999). Chemical reactions are initiated in crystalline solids when a crystal-specific threshold energy is exceeded. In this sense, initiation is linked to the rate of plastic deformation. However, practical energetic materials are usually heterogeneous composites comprised of one or more kinds of energetic crystals (the filler, for which the mass fraction can exceed 90%) bound together with a binder matrix that often consists of several different polymer, plasticizer, and stabilizer materials. Clearly, the mechanical behavior of these polymer-bonded (plastic-bonded) explosives (PBXs) is far more complicated than for neat crystals of high explosive. It is necessary in realistic constitutive modeling of energetic compositions to incorporate features reflecting the complex, multiphase, multiscale structural, dynamical, and chemical properties; see, for example, Bennett et al., 1998, and Conley & Benson, 1999. The goal in constitutive modeling is to bridge the particulate nature at the mesoscale to the mechanical properties at the macroscale.

The macroscale deformations applied to PBX composites in experiments are generally not the same as the local deformation fields in a component crystal within the composite. This has been demonstrated using grain-resolved mesoscale simulations wherein the individual grains and binder phases in a PBX are resolved within a continuum simulation framework.

Baer & Trott (2002) studied the spatial inhomogeneities in temperature and pressure that result when a shock wave passes through a sample of material. The statistical properties of the shocked state were characterized using temporal and spatial probability distribution functions of temperature, pressure, material velocity and density. The results showed that reactive waves in composite materials are distinctly different from predictions of idealized, traditional models based on singular jump state analysis.

Energy and stress localization phenomena culminating in rapid, exothermic chemistry are complex processes, particularly for shocks near the initiation threshold, for which subvolumes of material corresponding to the tails of the distribution functions of temperature and pressure are where initiation will begin. Therefore, a detailed understanding of composite energetic materials initiation requires knowledge of how thermal and mechanical energies are transferred through the various constituents and interfaces of a PBX; how the distributed energy causes structural changes associated with plasticity or phase transformations; and, when these processes (among others) lead to sufficiently high localization of energy, how and at what rate chemical reactions occur as functions of the local stress, temperature, and thermodynamic phase in the material. Each of these can in principle be studied by using molecular dynamics (MD) simulations. Distributions of field variables available from mesoscale simulations can be sampled to provide input to MD simulations; alternatively, results obtained from MD simulations can be used to guide the formulation of, and determine parameters for, improved mesoscale descriptions of the constituent materials in the PBX, for structurally perfect materials as well as ones containing various kinds of crystal lattice defects, voids, crystal surface features, and material interfaces (Kuklja & Rashkeev 2009; Sewell, 2008; Strachan et al., 2005; Shi & Brenner, 2008).

This chapter gives an overview of simulations of deformation processes in energetic materials at the macro-, meso-, and molecular scales. Both non-reactive and reactive processes are considered. Macroscale simulations are usually developed to mimic real life situations (for example, munitions performance under intended conditions or response under accident scenarios) or are used in the development of small-scale experiments designed to elucidate fundamental properties and behaviors. Because macroscale simulations lack detailed information concerning microscopic physics and chemistry, their use for predicting energetic materials initiation is generally limited to engineering applications of the types mentioned above. For many applications, however, the macroscopic treatment is sufficient to characterize and explain the deformation behavior of PBXs. At the other extreme of space and time scales, MD can be used to simulate the fine-scale details of deformation, including detailed mechanisms of phase changes, chemistry, and processes that occur at material interfaces or other spatial heterogeneities. Mesoscale simulation and theory is required to bridge the gap between these limiting cases.

The outline of the remainder of the chapter is as follows: First, the macroscopic deformation of a PBX, treated as a homogeneous material, is discussed. Specific examples are provided in which experimental data and simulation results are compared. Next, a sampling of the various approaches that can be applied for mesoscale modeling is presented. Representative simulations based on grain-resolved simulations are discussed. Finally, an overview of applications of molecular scale modeling to problems of thermal-mechanical-chemical properties prediction and understanding deformation processes on submicron scales is given, with specific references to the literature to highlight current capabilities in these areas.

2. Simulation of deformation at the macroscale: Plastic-bonded explosives treated as homogeneous material

The low-velocity impact vulnerability of energetic materials is typically studied by using simulations of deformations at the macroscale. For example, the engineering safety margin for acceptable crush-up limits of an encased energetic material is the most widely-used parameter in modern barrier design to prevent sympathetic detonation in ammunition storage sites. The accidental detonation of a storage module will lead to blast, ground shock, and propulsion of the barriers placed around that storage module. These accelerated barriers can impact adjacent storage modules and crush the munitions contained therein. The development of munition-specific acceptance criteria (Tancreto et al., 1994), and the comparison of double flyer-plate impact and crush-test results with simulation results (Malvar, 1994) helped advance the successful design of the so-called High Performance Magazine (Hager et al., 2000). Munitions are nowadays categorized into sensitivity groups based on robustness and sensitivity. The initiation threshold of a sensitivity group is expressed as the required kinetic energy and impulse per unit area from an impacting barrier to cause a reaction in munitions of that sensitivity group.
The concept of sensitivity groups allows for the design of other storage configurations through engineering models. One example is the simulation of barrier propulsion by the detonation of a single storage module containing 5 ton TNT equivalent of explosives, for which simulated results have been verified experimentally (Bouma et al., 2003; van Wees et al., 2004); see Fig. 1. However, design parameters related to the barrier do not describe the processes that may lead to ignition, and certainly do not help in formulating insensitive explosive compositions.

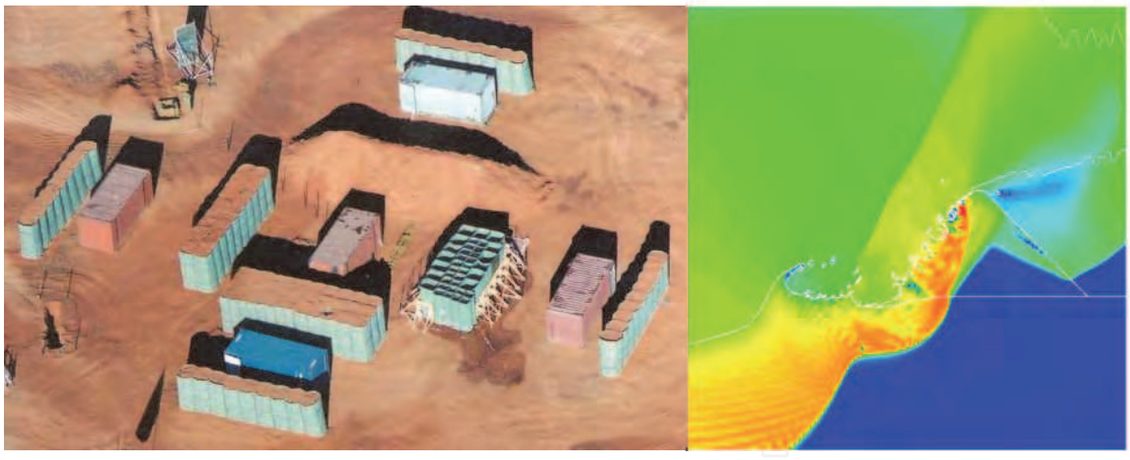

Fig. 1. Left: Experiment prior to detonation of 5 ton TNT equivalent of explosives in the central 24 ft container, which is surrounded by four different barrier designs and four munition storage modules. Right: The simulated results illustrate the pressure contours 5 ms after the detonation of 5 ton TNT equivalent of explosives, and the disintegration and movement of the trapezoid-shaped barrier in the photograph towards an adjacent storage module.

Many experimental tests, including the Susan impact test and friability test (UN, 2008), Steven impact test (Chidester et al., 1998), set-back generator (Sandusky et al., 1998), spigot intrusion (Wallace, 1994), drop-weight and projectile impact, and split Hopkinson pressure

bar (Siviour et al., 2004), study the response of a PBX under mechanical loading conditions that are specific to particular accident scenarios. Collectively, these tests span a wide range of geometric complexity and data richness. For some of them the results are expressed in relatively qualitative terms; for example, the Steven test where the severity of the mechanical insult to a stationary target with high explosive is based on the impact velocity of a projectile, and reaction violence is based on criteria such as amount of PBX recovered, damage to the target containment, and blast pressure at some distance from the location of projectile/target impact. In other tests more sophisticated experimental methods and highly instrumented diagnostics allow the detailed mechanical behavior to be inferred from the data; for example, the split Hopkinson pressure bar. In many cases simulations are required to aid in the interpretation of the data; specific examples for the split Hopkinson pressure bar, Steven impact, and LANL impact tests can be found in (Bailly et al., 2011; Gruau et al., 2009; Scammon et al., 1998).

The ballistic impact chamber is a specific drop-weight impact test designed to impose a shear deformation in a cylindrical sample of explosive (Coffey, 1995). (The name drop-weight impact test originates with the fact that the impact velocity depends on the height from which the weight is dropped onto the sample.) If a relationship between energy dissipation and rate of plastic deformation is known, the deformation rate can be used to define a mechanical initiation threshold (Coffey & Sharma, 1999). A drop-impact load impinges on the striker, which loads a cylindrical sample between the striker and an anvil (see Fig. 2) The cylinder is compressed along the cylinder axis and expands radially. The shear rate in the ballistic impact chamber is described by

$$\frac{d\gamma}{dt} \approx \frac{r_{t=0}}{h^2}\sqrt{\frac{h_{t=0}}{h}}\frac{dh}{dt}, \tag{1}$$

with r and h the radius and the height of the sample, respectively, $\gamma$the shear, and t the time. The shear rate is largest near the perimeter of the cylinder. Initiation is detected by photodiodes. Knowing the striker velocity dh/dt and the time of initiation, the required shear rate for initiation $d\gamma/dt$ can be calculated. Measured shear rate thresholds are given by Namkung & Coffey (2001).

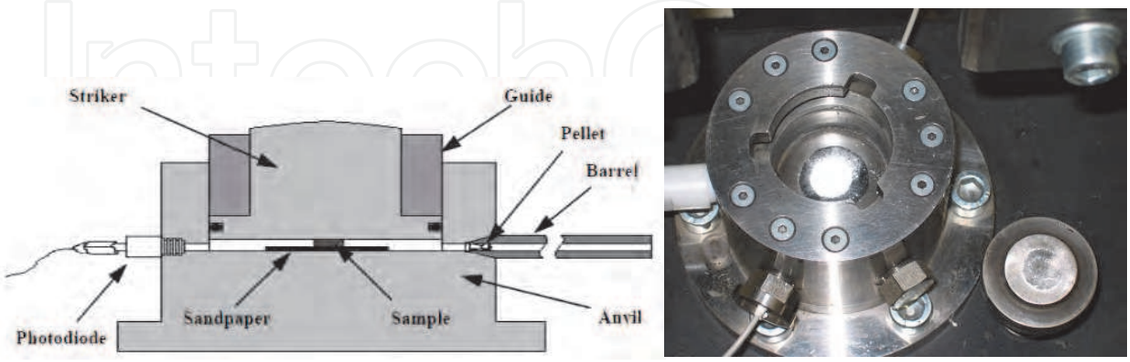

Fig. 2. Left: Schematic cross section of the ballistic impact chamber. Right: Top view of the chamber. The sample can be seen in the center of the chamber. Attached to the side are two fiber optic cables and a pressure transducer. The striker is located to the right of the chamber assembly.

The deformation of energetic materials in the ballistic impact chamber according to equation 1 has been verified by simulations of a cylindrical sample of PBXN-109 (64 wt% cyclotrimethylene trinitramine, 20 wt% aluminium and 16 wt% polybutadiene-based binder), 6.35 mm in diameter and 1.75 mm in height (Meuken et al., 2006). In this example, the drop weight had an impact velocity of 3 $m \cdot s^{-1}$, and the striker achieved an initial velocity of ≈ 6 $m \cdot s^{-1}$ due to elastic collision. The simulation was carried out using the ANSYS Autodyn software suite, a versatile explicit analysis tool for modeling the nonlinear dynamics of solids, fluids, gases and interactions among them. (Autodyn provides, for example, finite element solvers for computational structural dynamics and mesh-free particle solvers for high velocities, large deformation and fragmentation (Autodyn, Birnbaum et al., 1987).) The resulting shear rate in PBXN-109 as a function of time is shown in the right-hand panel of Fig. 3. The maximum shear rate of approximately 8×10^5 s^{-1} is reached shortly before the end of the negative acceleration of the striker, at a radial distance about 70% of the sample radius (Bouma et al., 2007). The shear rate values from equation 1 and the Autodyn simulation are comparable, except the rise in shear rate in the simulation occurs at a longer time since impact. The deformation is complex – there are small oscillations visible in Fig. 3 due to the shock and reflection waves that travel through the striker and anvil. Evaluation of the shear sensitivity according to equation 1 is non-trivial, and simulations are key to interpreting this "simple" cylindrical compression experiment. The analysis requires that the sample not resists compression by the striker prior to initiation and that an accurate value of the striker velocity is known. In the example discussed here the first requirement is satisfied so long as the time to reaction is less than 90% of the original sample height divided by twice the drop weight velocity at the moment of impact. The experimentally determined shear initiation threshold in the ballistic impact chamber of PBXN-109 is 1.7×10^5-2.0×10^5 s^{-1}. A simulation that approximates the experimental conditions and which includes chemical reaction yields an ignition time of 180 μs. The chemical reaction model used in the simulation is limited to an Arrhenius-type ignition term; a more sophisticated treatment of chemistry that includes, for instance, the Lee-Tarver (Lee & Tarver, 1980) growth term has not been performed (Zerilli et al., 2002).

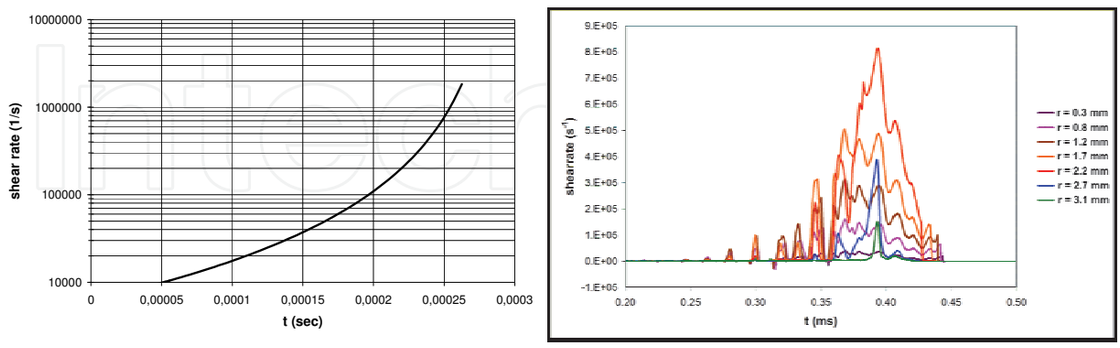

Fig. 3. Left: Shear rate vs. time, calculated using equation 1. The deformation starts at $t = 0$ and is monitored until the height of the sample is equal to 10% of the initial height. Right: Same as the left-hand panel except the result is obtained from an Autodyn simulation. Results in the right-hand panel are shown for points near the sample-anvil interface and originally located at radial distances r = 0.3, 0.8, 1.2, 1.7, 2.2, 2.7, and 3.1 mm from the center of the sample; deformation of the sample starts at t = 0.07 ms.

The shear-rate threshold just discussed should also apply to other experimental configurations. For example, PBXN-109 has been subjected to an explosion-driven deformation (Meuken et al., 2006). Steel cylinders were filled with PBXN-109 and a layer of 3.0, 4.0, or 5.0 mm plastic explosive, covering one-third of the circumference of the steel cylinder, was detonated; the results are shown in Fig. 4. In the 3-mm layer case the PBXN-109 was slightly extruded from the deformed steel cylinder without any sign of reaction. In the 4-mm layer case there was a mild reaction, as shown by the slightly expanded steel cylinder. In the 5-mm layer case a violent reaction of the PBXN-109 was observed, resulting in fragmentation of the steel cylinder.

Figure 5 shows the 2-D simulation set-up of the deformation experiment (left panel); as well as the shear rate (right panel) in the PBXN-109, calculated close to the inner surface of the steel cylinder as a function of the angle (where angle θ=0° corresponds to the center of the deformation layer). The maximum shock pressure is ≈0.5 GPa, which is well below the 2.2-5.2 GPa initiation pressure of PBXN-109 in the large scale gap test (Doherty & Watt, 2008). The maximum shear rates in Fig. 5 are 0.72×10^5, 1.19×10^5, and 1.51×10^5 s^{-1}, respectively, for the 3-, 4-, and 5-mm layer experiments. The initiation threshold in this deformation test resembles the threshold in the ballistic impact chamber.

Fig. 4. Explosion-driven deformation of steel-cased PBXN-109 charges. The deformation results from the detonation of a layer of plastic explosive that partially surrounds the PBX-N109 charges (see Fig. 5). Results are shown for plastic explosive layer thicknesses of 3 mm (left), 4 mm (middle) and 5 mm (right).

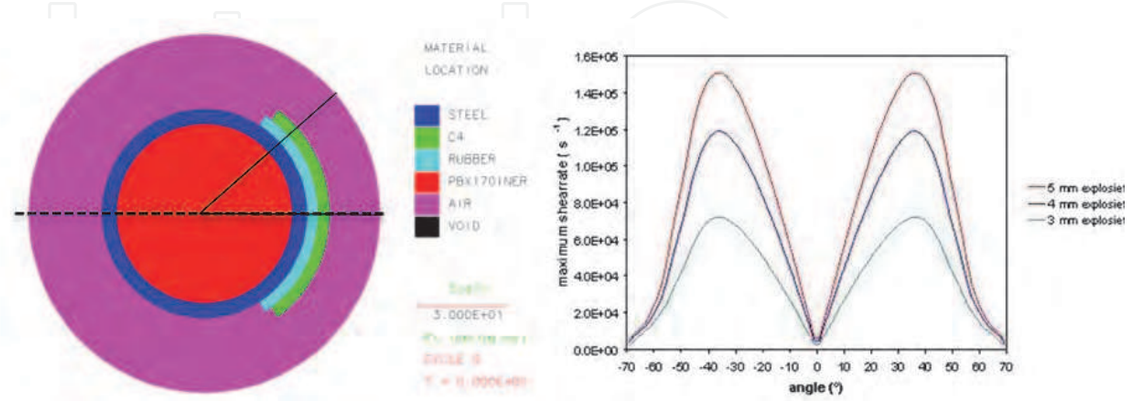

Fig. 5. Left: Schematic configuration for 2-D Autodyn simulation of an explosive deformation test. Right: Maximum shear rates in PBXN-109 as functions of the angle θ when deformed by explosive layers of thickness 3 mm (green), 4 mm (blue), and 5 mm (red).

The maximum shear rate depends on the test configuration. The friability test (UN, 2008) and the LANL impact test (Bennett et al., 1998) have been simulated for the explosive PBXN-109, and the Steven impact test (Vandersall et al., 2006) for explosive composition C4, to correlate the severity of mechanical deformation to initiation of the explosive, see table 1 (Bouma & Meuken, 2004). Permanent deformation and extensive fracturing of the PBX in the friability test, in which a flat-ended cylindrical projectile is fired into a rigid steel target, are evident in Fig. 6 (left-hand panel, from Bouma, 1999) as well as the simulated evolution of shear rate (right-hand panel). The largest calculated shear rate, ~0.45×10^5 s^{-1}, occurs near the edges of the ∅18 mm sample. The experimental result in the left-hand panel of Fig. 6 shows that this rate is too low to cause initiation; this is qualitatively consistent with the threshold maximum shear rates discussed in connection with Figs. 3-5. The extensive fracture of the material, which is deliberately induced in this test, has not been modeled.

Fig. 6. Left: Permanent deformation and fracture of a PBX containing 80% HMX at 91, 110, 121, and 154 $m{\cdot}s^{-1}$ impact velocity in a friability test. Right: The evolution of shear rate at various radial distances from the sample in the friability test and near the explosive/steel interface for PBXN-109 at 150 $m{\cdot}s^{-1}$ impact velocity. The maximum shear rate develops near the outer radius.

The Steven impact test has been simulated near the experimental initiation thresholds for explosives PBX 9404 and PBX 9501, respectively 31-34 $m{\cdot}s^{-1}$ and 39-54 $m{\cdot}s^{-1}$ (Chidester et al., 1998). Again, the calculated shear rates of $\approx10^5$ s^{-1} confirm experimental initiation thresholds. Note that the experimental threshold for C4 is an impact velocity of more than 195 $m{\cdot}s^{-1}$ (Vandersall et al., 2006), resulting in a shear rate of at least 1.8×10^5 s^{-1}. In the LANL impact test a pusher impacts a thin rectangular slab of explosive of the same thickness (Bennett et al., 1998). The violence of reaction depends on the diameter and shape of the pusher (result not shown). The calculated peak shear rate of 16×10^5 s^{-1} is large but is very localized, within 1 mm of the edge of the ∅10 mm pusher, and has duration <1μs.

An analytical model has been developed that links mechanical properties and particle sizes with the thermal ignition of an explosive. This micro-structural model (Browning, 1995) is based on 1) Hertz contact stress between two particles of the same diameter in relation to the applied normal pressure, 2) mechanical work due to sliding motion under a normal pressure, and 3) thermo-chemical decomposition due to an applied and local heat flux (the latter originating from the mechanical work in the Hertzian contact points). The ignition criterion in the model requires the evaluation of the pressure and the shear rate at the macroscale (Browning, 1995; Gruau et al., 2009; Scammon et al., 1998). Scammon et al. (1998) evaluate the parameter

$$p^{2/3}\left(\frac{d\gamma}{dt}\right)_{max}^{1.27} t_{ign}^{1/4} \tag{2}$$

Configuration, explosive	Test specifics	Shear rate / s^{-1}	Experimental observation
Explosion driven deformation, PBXN-109	3 mm deformation layer 4 mm deformation layer 5 mm deformation layer	Max. 0.72×10^5 Max. 1.19×10^5 Max. 1.51×10^5	No reaction Burn Violent reaction
Ballistic Impact Chamber, PBXN-109		1.7×10^5-2.0×10^5 at initiation	Initiation
Friability test, PBXN-109	18 mm Ø, 9 gram, 150 $m\cdot s^{-1}$ impact velocity	Max. 0.4×10^5-0.5×10^5	No reaction
LANL impact test, PBXN-109	10 mm blunt steel pusher at 196 $m\cdot s^{-1}$ into 25 mm ×20 mm sample	Max. 16×10^5	Not available
Steven impact test, C4	50 $m\cdot s^{-1}$ impact velocity 100 $m\cdot s^{-1}$ impact velocity 157-195 $m\cdot s^{-1}$ impact velocity	Max. 0.5×10^5 Max. 1.8×10^5	No reaction

Table 1. Comparison of shear rates calculated in simulation of various test configurations of PBXN-109 and explosive composition C4 to experimental results.

with time to ignition t_{ign}, assuming that pressure p and shear rate $d\gamma/dt$ are constant. Ignition is associated with the parameter exceeding an explosive-specific value. The underlying thermo-chemical model has been analyzed in detail for HMX only. However, equation 2 (or the corresponding expression for variable pressure and shear strain rate loading histories (Browning & Scammon, 2001; Gruau et al., 2009)), may not be directly applicable to non-HMX PBXs. The thermo-chemical decomposition in the above model requires a thermo-chemical simulation of the ignition time as a function of thermal energy fluence through a crystal-crystal contact surface area, and involves explosive-specific decomposition chemistry that can be measured, for example, in a one-dimensional time-to-explosion (ODTX) test (Hsu et al., 2010). This may lead to different exponents in eq. 2 for non-HMX PBXs.

As shown in this section, a macroscopic treatment is generally sufficient to characterize and explain the deformation behavior of PBXs. However, since macroscopic models treat the PBX as a homogeneous material, their use for predicting energetic materials initiation is rather limited. As a first step to a more detailed description of the deformation and initiation behavior of energetic materials, mesoscale simulations can be performed that include the influence of the particulate nature of PBX formulations.

3. Simulation of deformation at the mesoscale: The influence of particulate nature of plastic-bonded explosives

The influence of the particulate nature at the mesoscale can be accounted for in different ways. One can 1) fit a continuum model with particle-specific features to experimental data; 2) simulate the mechanical behavior of a representative volume element with the mechanical

properties of its constituents and determine the collective mechanical behavior; or, 3) when sufficient computer resources are available, simulate the mechanical behavior with spatially resolved explosive grains and binder.

An example of the first approach is based on the statistical crack mechanics model (Dienes, 1985) in combination with a five-component Maxwell visco-elasticity model, fitting the parameters to experimental Young's moduli spanning eight orders of magnitude of relaxation times (Bennett et al., 1998). Constitutive equations are obtained for implementation into the DYNA3D nonlinear, explicit finite element code for solid and structural mechanics (DYNA3D). An example of the second approach is the construction of a continuum constitutive model based on homogenization procedures applied to realistic 2-D or 3-D representative volume element microstructures obtained, for instance, from digital images of cross sections (De & Macri, 2006) or X-ray microtomography (Bardenhagen et al., 2006) of a PBX. An example of the third approach is the direct simulation at the mesoscale of the propagation of a shock wave through randomly packed crystal ensembles (Baer & Trott, 2002). Probabilistic distribution functions of wave field variables such as pressure, density, particle velocity, chemical composition, and temperature are studied to gain insight into the initiation and growth of reactions in heterogeneous materials. For additional studies of grain-resolved systems see Baer (2002), Reaugh (2002), and Handley (2011); the latter is a recent Ph.D. dissertation that includes a thorough review of mesoscale simulations and theory applied to PBXs.

During mechanical deformation of a PBX interfacial de-bonding can occur and crystals may even crack. Figure 7 contains a scanning electron micrograph of HMX crystals in a hydroxy-terminated-polybutadiene binder. A cylindrical sample of this explosive, 9 grams in weight and 18 mm in diameter, has been impacted at 92 $m \cdot s^{-1}$ against a steel plate. The micrograph corresponds to a section near the impact site in the friability test and demonstrates interfacial de-bonding as well as crystal cracking (Scholtes et al., 2002). These phenomena can also be simulated. Figure 8 gives the principal stress in uniaxial compression of PBX 9501 at 2% overall strain. The computational model is 0.465 mm × 0.495 mm and contains 25 particles. De-bonding occurs when the work applied perpendicular or tangential to an interface exceeds the normal or shear cohesive energy, respectively. The cohesive energies used to generate the left- and right-hand panels of Fig. 8 are, respectively, below and above the experimentally derived values. The extent of interfacial de-bonding decreases with increasing cohesive energy between the particle and binder phases. The increase in cohesive energy results in a large stress localization within crystals, which increases the probability for cracks to develop within the crystal (Yan-Qing & Feng-Lei, 2009). Note that the peak shear rates in the impact experiment of Fig. 7 are of the order of 10^3 s^{-1}, whereas the simulation results shown in Fig. 8 are for a strain rate of 1.2×10^{-3} s^{-1}.

The particulate nature of most energetic materials and the imperfection of the component crystals (for example, grain boundaries, seeding crystals, voids, cracks, lattice defects, solvent inclusions) not only influence the deformation behaviour of the PBX but also the sensitivity to shock (Doherty & Watt, 2008; van der Heijden & Bouma, 2004a, 2004b, 2010). Examples of imperfections are shown in Figs. 9 and 10. On the left is an optical micrograph of a cross section of an RDX crystal. The crystal outer surface is irregular, grains have grown into each other, and there are multiple defects with sizes of the order of 10 μm. On the right a scanning electron micrograph of the cross section of an RDX crystal from the same lot (RDX type II obtained from Dyno) is shown. At this magnification, one can see voids with

sizes on the order of hundreds of nm, as well as a string of voids extending vertically across the image; note that this latter structure is not a grain boundary. Fig. 10 shows two confocal scanning laser micrographs with a Dyno Type II RDX crystal at the left and a BAe Royal Ordnance RDX crystal at the right. By using a confocal scanning laser microscope in reflection mode it is possible to make optical slices from a transparent object down to a thickness of about 0.5 μm. In this way, local differences in the refractive index inside a crystal will be revealed as bright spots on a dark background. The images are recorded with a Leica TCS SL confocal system using a DM6000 B microscope equipped with a 40X objective, zoom factor setting of 2. The spots indicate locations with a different refractive index from the surrounding area and correspond most likely to small inclusions present in the crystal. Also of interest are the "diffuse" areas within the crystals in the left-hand panel of Fig. 10. The differences in spot density for the two RDX lots obtained from different producers are assumed to be correlated with the difference in mechanical sensitivity (Thompson et al., 2010) and shock sensitivity (Doherty & Watt, 2008).

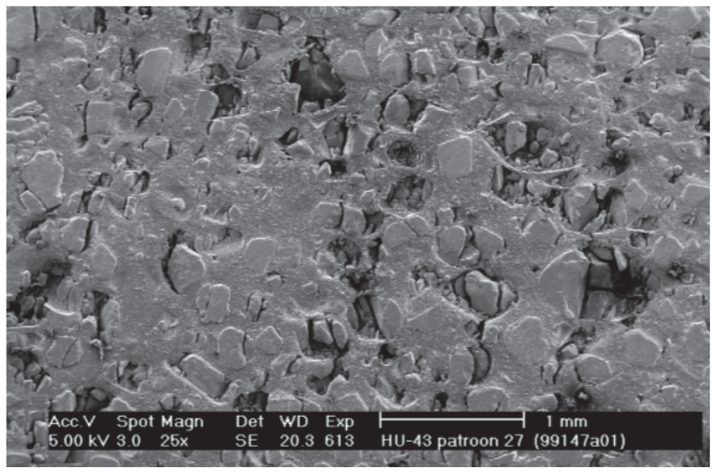

Fig. 7. Interfacial debonding and crystal cracking in a friability test (Scholtes et al., 2002).

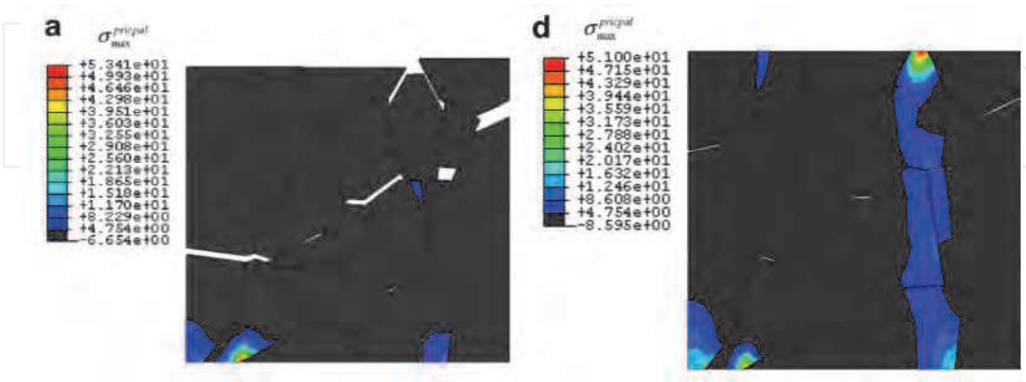

Fig. 8. Maximum principal stress in uniaxial compression of PBX 9501 (Reprinted from Yan-Qing & Feng-Lei, 2009, © 2008, with permission from Elsevier). The two simulations are identical except that the particle/binder cohesive energy used to generate the right-hand panel is four times that used to generate the left-hand panel.

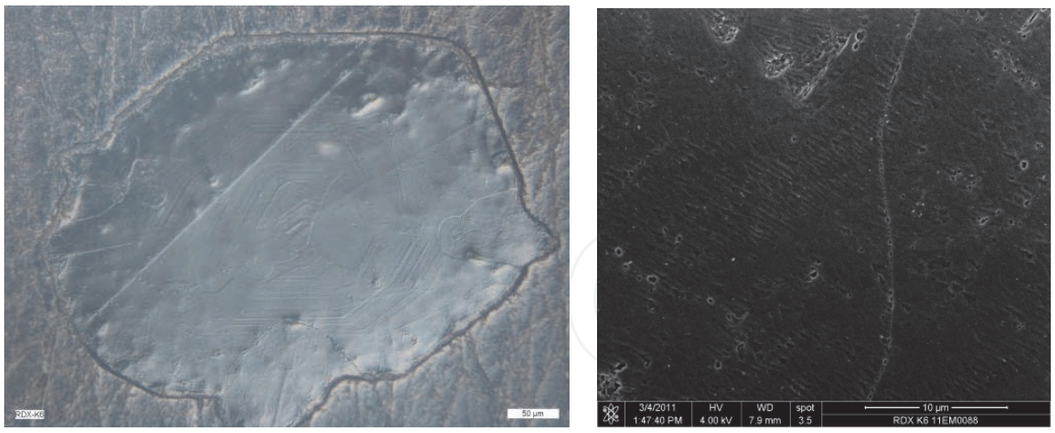

Fig. 9. Optical micrograph (left) and scanning electron micrograph (right) of a cross-section of a crystal of Dyno type II RDX (Thompson et al., 2010).

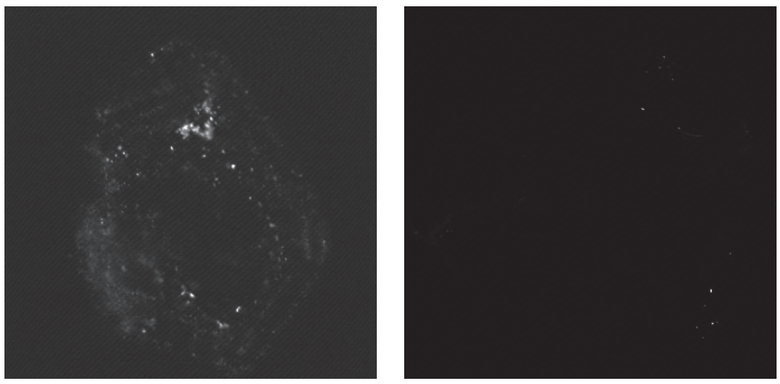

Fig. 10. Confocal scanning laser micrographs for two different qualities of RDX crystals, produced at a focal plane below the surface. Left: 93.5 μm × 93.5 μm image of Dyno type II RDX. Right: a 375 μm × 375 μm image of BAe Royal Ordnance RDX (Thompson et al., 2010).

Ideally, a simulation at the meso- or molecular-scale should incorporate microstructural features such as grain boundaries, packing of particles, defects, and voids. A new method to create a computational set-up with a random pack of arbitrary shapes of particles has been applied to "typical" HMX crystals by Stafford & Jackson (2010). Armstrong (2009) has reviewed dislocation mechanics modeling of energetic materials. The review covers experimental mechanics studied through indentation-hardness properties, impact properties in various test geometries, and granular compaction. The thermal dissipation of energy is associated with individual dislocation motions, which may induce a strong adiabatic heating through dislocation pile-up avalanches. Lei and Koslowski (2010) have published a phase field dislocation dynamics model for low-symmetry organic crystals. Using only information about the crystallography and elastic constants they were able to predict the onset of plastic deformation in sucrose and paracetamol. (Although these are not energetic materials, the fundamental physics and materials science developed by Lei and Koslowski would apply equally well to energetic crystals.) Lei and Kowslowski identified several properties that could be provided from atomic-scale simulations. The use of MD simulations as a means of providing input to, or guiding the formulation of, mesoscale models will be discussed in the next section.

4. Simulation of deformation at the molecular scale: Structural changes and chemical reactions near lattice defects, voids, and interfaces

Atomic-level simulation methods — MD and Monte Carlo (MC) — in which individual atoms or chemical functional groups are treated explicitly can be used to understand and predict the equilibrium and dynamic properties of energetic crystals, binders, and interfaces between them. In MD a set of classical (e.g., Newton's) equations of motion are solved in terms of the interatomic forces, possibly with additional terms corresponding to coupling of the system to an external thermostat (Hoover, 1985; Nosé, 1984), barostat (Martyna et al., 1996; Parrinello et al., 1981), or other constraint such as to sample a Hugoniot state of a material (Maillet & Stoltz, 2008; Ravelo et al., 2004; Reed et al., 2003) to confine the simulation to a particular ensemble, leading to a trajectory (time history) of particle positions and momenta from which physical properties can be calculated in terms of appropriate statistical averages or time correlation functions (Tuckerman, 2010). The interatomic forces required for MD can be obtained from a parameterized empirical force field or from electronic structure calculations wherein the forces are obtained directly from the instantaneous electronic wave function of the system.

Monte Carlo sampling of configuration space is usually performed using a random walk based on a Markov chain constructed to satisfy microscopic reversibility and detail balance in an appropriate statistical ensemble. (See, for example: Frenkel & Smit, 2002; Wood, 1968.) Because the sequence of states in a Markov chain does not comprise a dynamical trajectory, only properties that can be expressed as averages of some microscopic function of configuration in phase space that does not explicitly involve the time can be computed. Metropolis MC (Metropolis et al., 1953), the version of MC most frequently used in molecular simulations, does not require evaluation of forces but rather only differences in potential energy between adjacent states (configurations) sampled by the Markov chain. Although in many cases MC and MD can be used equally effectively, in practice Monte Carlo is not used as widely as MD in simulations of energetic materials; therefore here we focus on MD.

Electronic structure calculations are sometimes used to study the structures, energies, charge distributions and higher multipole moments, spectroscopy, and reaction pathways. These properties can be calculated for isolated molecules, clusters, or periodic structures, usually at zero Kelvin; however, the effects of finite temperature can be incorporated, for example, by using the quasi-harmonic approximation (for example, Zerilli & Kukla, 2007), explicitly from MD trajectories, (Manaa et al., 2009; Tuckerman & Klein, 1998) or using an appropriate MC sampling scheme (Coe et al., 2009a, 2009b). Most practical electronic structure calculations for energetic materials are performed using methods based on the Kohn-Sham density functional theory (DFT) (Koch & Holthausen, 2001), although *ab initio* methods are used in some cases (Molt et al., 2011).

The advantage of atomic-level simulation methods is the detailed information they can provide. For instance, a MD simulation provides the time histories of the phase space coordinates along a trajectory, from which any classical property of the system, including detailed reaction chemistry can, in principle, be computed. The main obstacle to the use of atomic methods in practical multi-scale simulation frameworks is the small spatiotemporal scales that can be studied — approximately tens of millions of atoms for time scales of nanoseconds or less — and the requirement, at least for accurate studies rather than ones designed to examine basic qualitative features of the material response, to have a reliable description of the inter-atomic forces within the given thermodynamic regime of interest.

(While the development of parallel, linear scaling algorithms for electronic structure studies of condensed phase systems has considerably increased the numbers of atoms that can be studied (see, for example, Bock et al., 2011; Kresse et al., 2011), system sizes and simulation times tractable based on electronic structure theory calculations are far smaller than those using analytical force fields.) A more fundamental question in the case of MD or MC simulations is that of the applicability of classical statistical mechanics or dynamics for the study of molecular phenomena.

In the following we discuss ways by which atomic-scale information can be incorporated within a multiscale simulation framework, providing specific examples relevant to energetic materials. The focus of most MD simulations of energetic materials has been on predicting physical properties in the absence of chemistry. A major (and ongoing) hurdle to reliably treating complex chemistry in MD simulations is the difficulty of describing the forces for the variety of electronic structures that would be explored at the high temperatures and pressures corresponding to the von Neumann spike or Chapman-Jouguet state of a detonating explosive. Currently, the methods to do this are plane-wave DFT or parameterized analytic representations such as the ReaxFF (van Duin et al., 2001; Strachan et al., 2005) or AIREBO (Stuart et al., 2000; Liu & Stuart, 2007) force fields. Han et al. (2011) have recently published simulations of the thermal decomposition of condensed phase nitromethane studied using ReaxFF.

In general, there are two approaches to the multiscale problem. The arguably simpler approach is a sequential (or "handshaking") one in which specific physical properties required in mesoscale or macroscopic simulations — for example, thermal, transport, or mechanical properties — are calculated as functions of temperature and pressure and used directly in the larger-scale simulations. Assuming the validity of classical mechanics, the major challenge to obtaining reliable predictions for such quantities is the need to realistically account for defect structures that can be of sizes that exceed the limited MD spatiotemporal scales. Reliable predictions of properties or structures of rate-dependent materials or ones with extended interfaces are also difficult to model due to the large time and space scales associated with them; for example, binders in energetic materials are usually based on polymers (often with other additives such as plasticizers or stabilizers) that exhibit both viscoelastic behavior and in some cases complex microphase-segregated morphologies and non-negligible concentration gradients in the neighborhood of interfaces. Such simulations are quite challenging within a MD framework; see, for example, Jaidann et al. (2009). Nevertheless, in some instances it is possible to regard MD predictions as comprising bounding cases (for example, limit of perfect crystals). Moreover, for many properties of interest experimental data either do not exist for conditions away from room temperature/atmospheric pressure or have large apparent uncertainties based on disparate results obtained for a given property using different experimental techniques. In such instances the results of atomic simulations can be used to extend the intervals over which needed parameter values can be estimated or to discriminate among inconsistent data sets.

Examples are included in Table 2, which includes the results of various measurements or calculations of the second-order elastic tensors for PETN, α-RDX, and β-HMX; and Table 3 which contains the pressure and temperature dependence of the bulk and shear moduli of crystalline TATB for the Reuss (uniform stress) and Voigt (uniform strain) bounds. Note the wide variation in some of the experimentally determined values, particularly for RDX and HMX. In each case, the MD results – based on force fields that were not parameterized using elasticity data – yield predictions in good agreement with the most recent, and presumably most accurate, experimental data based on impulsive stimulated thermal scattering.

A difficulty with direct application of sequential approaches is that, even if a given property appears in a mesoscopic theory and can be calculated directly and accurately using atomic methods, possibly including temperature and pressure dependencies, use of those accurate property values which are treated as adjustable parameters in mesoscale simulations may lead initially to decreased predictive capability compared to experimental results; that is, an improved subgrid model or more accurate physically-based parameter specification may disrupt the overall calibration of the mesoscale model.

The other general approach to multiscale simulation of energetic materials is the concurrent method in which two different levels of material description are included simultaneously within a single simulation domain. One example where such an approach would be useful is grain-resolved mesoscale simulations wherein regions of atomically resolved material are contained within a larger volume of material treated using continuum mechanics. Such an approach would be particularly useful for mesoscopic studies of the effects of intra-crystal defects (dislocations, grain boundaries, voids) or intermaterial interfaces (crystal-binder, High Explosive (HE)-metal) where localization of temperature, stress, or microscopic strain rate might be large leading to large gradients in the material (often called *hot spots*) wherein chemical reactions are likely to occur. In addition to theoretical difficulties with formulating a single simulation method in which particles and continuum regions are treated seamlessly, concurrent methods are difficult to implement due to the high degree of time sub-cycling required given the large difference between the time step in a MD simulation (~0.01-1 fs) compared to the time step in even a high resolution mesoscale simulation (~0.1 ns). Other possibilities for progress based on concurrent approaches include using different levels of description (and, tacitly assumed, different accuracies of forces) within a single MD computational domain; for example, use within a limited region such as the neighborhood of an interface of a force description based on electronic structure or empirically-calibrated force fields that include chemical reaction surrounded by a (typically much larger) region of material represented by a less accurate but computationally cheaper model (for instance one with fixed intramolecular connectivity that does not treat chemical reaction). Applications of the *computational materials design facility* (for example, Jaramillo-Botero et al., 2011 and references therein) illustrate the potential of such methods.

Another approach to extending the space and time scales accessible to molecularly-detailed methods that has been used with increasing frequency is particle-based coarse-graining in which chemical functional groups or entire molecules or collections of molecules are treated as effective particles, with corresponding effective potentials. As an example, Desbiens et al. (2007, 2009) have developed a model for nitromethane in which the four atoms of the methyl group are treated as a single particle. This simplified model has been parameterized using a MC optimization approach, and shown to yield good agreement with several measured quantities, including second shock temperatures. Gee and co-workers (Gee et al., 2006; Lin et al., 2007) have developed a coarse-grained description for PETN in which individual PETN molecules are represented by a five-bead model (nominally the tetramethyl carbon and the four nitrate pendent groups) (Gee et al., 2006), and have used this model to study surface diffusion of PETN molecules on different PETN crystal faces (Lin et al., 2007). Izvekov et al. (2010) have developed a formalism for systematic coarse-graining of molecular materials and applied it to nitromethane; both a one-site model, in which the molecules are treated as single particles, and a two-site model, in which the methyl group and nitro groups are treated as distinct particles, were developed. The approach, which is based on a systematic calibration of effective coarse-grained particle-particle interactions using potential-of-mean-force calculations for fully atomic systems, was shown in the case of a density-dependent potential

formulation to reproduce the nitromethane liquid structure and shock Hugoniot locus. Lynch et al. (2008) have developed a simplified model for α-HMX in which individual molecules are treated as single particles; a novel aspect of this reduced dimensionality "mesodynamics" (Strachan & Holian, 2005) potential function is that it includes the effects of intramolecular vibrational degrees of freedom through incorporation of implicit degrees of freedom. The model, which is only intended to provide a schematic representation of HMX, has been used to study spall behavior in the shocked crystals. With all coarse-graining or multiscale methods, a key requirement is to capture the dominant features of the physics at the finer scale when passing from one scale to the next larger one, and to minimize the amount of non-essential information that is carried along. The specific requirements will vary depending on the material type, the thermodynamic and mechanical loading regime of interest, and the fidelity of the higher-scale model in which the finer-scale results are to be used.

	C_{11}		C_{33}	C_{44}		C_{66}	C_{12}	C_{13}					
PETN													
Ultrasonics[a]	17.22		12.17	5.04		3.95	5.44	7.99					
ISTS[b]	17.12		12.18	5.03		3.81	6.06	7.98					
MD/MC[c]	17.6		10.5	4.66		4.92	4.7	6.65					
	C_{11}	C_{22}	C_{33}	C_{44}	C_{55}	C_{66}	C_{12}	C_{13}	C_{23}				
RDX													
MC[d]	26.9	24.1	17.7	8.4	5.3	7.6	6.27	5.68	6.32				
Ultrasonics[e]	25.02	19.6	17.93	5.17	4.07	6.91	8.2	5.8	5.9				
Brillouin[f]	36.67	25.67	21.64	11.99	2.72	7.68	1.38	1.67	9.17				
RUS[g]	25.6	21.3	19.0	5.38	4.27	7.27	8.67	5.72	6.4				
ISTS[b]	25.15	20.08	18.21	5.26	4.06	7.10	8.23	5.94	5.94				
Energy Minimized[h]	25.0	23.8	23.4	3.1	7.7	5.2	10.6	7.6	8.8				
	C_{11}	C_{22}	C_{33}	C_{44}	C_{55}	C_{66}	C_{12}	C_{13}	C_{23}	C_{15}	C_{25}	C_{35}	C_{46}
β-HMX													
ISLS[i]	20.8	---	18.5	---	6.1	---	---	12.5	---	-0.5	---	1.9	---
Brillouin[j]	18.41	14.41	12.44	4.77	4.77	4.46	6.37	10.50	6.42	-1.10	0.83	1.08	2.75
ISTS[k]	20.58	19.69	18.24	9.92	7.69	10.67	9.65	9.75	12.93	-0.61	4.89	1.57	4.42
MD/MC[l]	22.2	23.9	23.4	9.2	11.1	10.1	9.6	13.2	13.0	-0.1	4.7	1.6	2.5

a. Winey & Gupta, 2001.
b. Sun et al., 2008. ISTS: Impulsive stimulated thermal scattering.
c. Borodin et al., 2008. Composite MD/MC simulations using flexible molecules.
d. Sewell and Bennett, 2000. MC simulations using rigid molecules.
e. Haussuhl, 2001. The crystal axes used in the original publication have been transformed to coincide with that used here.
f. Haycraft et al., 2006.
g. Schwarz et al., 2006. RUS: Resonant ultrasound spectroscopy.
h. Munday et al., 2011. Molecular mechanics using flexible molecules.
i. Zaug, 1998. Partial determination. ISLS: Impulsive stimulated light scattering.
j. Stevens & Eckhardt, 2005.
k. Sun et al., 2009.
l. Sewell et al., 2003.

Table 2. Second-order elastic coefficients of PETN, RDX, and β-HMX determined using various methods. Units are GPa.

Pressure (GPa)	K_{Reuss}	K_{Voigt}	G_{Reuss}	G_{Voigt}
0.0	13.2	20.3	1.8	11.5
4.0	46.1	62.7	5.2	27.9
8.0	73.3	97	6.5	37.9

Table 3. Calculated pressure-dependent Reuss average and Voigt average bulk and shear moduli for TATB crystal. Units are GPa. The temperature is T = 300 K. (Adapted from Bedrov et al., (2009).)

Menikoff & Sewell (2002) have reviewed the physical properties and processes needed for mesoscale simulations of HMX. Among the properties required that can be reliably computed for pure materials using atomic-level modeling methods are the thermodynamic phase boundaries between the polymorphic forms of the crystal and the melting point as a function of pressure; the coefficients of thermal expansion and isothermal compression; the heat capacity as a function of temperature and, in general, pressure; the modal and volumetric Gruneisen coefficient; the elastic tensor and derived isotropic moduli as functions of temperature and pressure; the elastic-plastic yield surface, which in general is temperature and stress dependent, and may also exhibit a strain-rate dependence; and thermal conductivity and shear viscosity as functions of pressure and temperature. A number of these properties have been computed for HMX and used in continuum simulations: the elastic tensor (Sewell et al., 2003; Barton et al., 2009; Zamiri & De, 2010), the temperature-dependent shear viscosity of the liquid (Bedrov et al., 2000; Dienes et al., 2006), the temperature-dependent specific heat (Goddard et al., 1998; Sewell & Menikoff, 2004), Other properties discussed by Menikoff and Sewell that must be considered in a realistic simulation are the "damage" state of the material, for instance size and distributions of cracks; the nature and density of defects within the crystals; and the effects of material interfaces on the composite behavior. Bedrov et al. (2003) have discussed how some of these properties can be obtained from MD simulations. More recently, Rice and Sewell (2008) reviewed atomic-scale simulations of physical properties in energetic materials, with a focus on predictions of properties for systems in thermal equilibrium.

Single-crystal plasticity of RDX has been studied using atomic-level simulation methods and, in some cases, compared to experimental results. Cawkwell and co-workers (Cawkwell et al., 2010; Ramos et al. 2010) have used MD simulations of the shock response of initially defect-free (111)- and (021)-oriented RDX single crystals to interpret the "anomalous" elastic-plastic response observed in flyer plate experiments for that orientation, wherein the evolution with increasing impact strength of VISAR velocity profiles for the (111) orientation transforms from a clear two-wave elastic-plastic structure to a nearly-overdriven structure over an interval of shock pressures that is narrow compared to the results obtained for other crystal orientations. The MD results show that, above a well-defined threshold shock strength, stacking faults nucleate homogeneously in the material then rapidly propagate, leading to mechanical hardening consistent with the abrupt transition from a two-wave structure to a nearly overdriven one (Cawkwell et al., 2010). Based on the results for the (111)-oriented crystal, Ramos et al. (2010) predicted that similar behavior should arise for shocks in (021)-oriented RDX, a result that was confirmed both from MD simulations and flyer plate experiments. Chen et al. (2008) performed large-scale MD simulations of nanoindentation of (100)-oriented RDX crystal by a diamond indenter using a version of the ReaxFF reactive force field **(**van Duin et al., 2001; Strachan et al., 2005). They observed localized damage in the region of the indenter, and calculated a material hardness that is

consistent with experimental data. They concluded that dominant slip occurs in the (210) plane along the $[\bar{1}20]$ direction. Ramos et al. (2009) have reported atomic-force microscopy/nanoindentation experiments for oriented RDX crystals. Because Ramos et al. did not study indentation for the (100) surface, a direct comparison between their data and the MD results of Chen et al. is not possible.

Energetic material crystals (and organic crystals generally) often crystallize into low-symmetry space groups, exhibit polymorphism (*c.f.*, the multiple crystal phases of HMX (see Refs. 2-5 in Sewell et al., 2003) and RDX (Millar et al. (2010), and references therein; and Munday et al. (2011))), and are often highly anisotropic in terms of thermal, mechanical, and surface properties (the graphitic-like stacking of layers in TATB crystal provides an extreme case (Kolb & Rizzo, 1979; Bedrov et al., 2009). This can lead to anisotropic elastic-plastic shock response (Hooks et al., 2006; Menikoff et al., 2005; Winey & Gupta, 2010) and even anisotropic shock initiation thresholds, as has been shown by (Dick, 1984; Dick et al., 1991, 1997) for the case of PETN crystal.

A number of MD studies have been performed to assess shock-induced phase transitions, anisotropic shock response, and effects of crystal surface properties on polymer adhesion properties. Thompson and co-workers have studied melting in RDX, and noted a structural transition that occurs for temperatures just below the melting point (Agrawal et al, 2006). Thompson and co-workers have also studied the melting (Agrawal et al., 2003; Zheng et al., 2006; Siavosh-Haghighi, 2006) and crystallization (Siavosh-Haghighi et al., 2010) of nitromethane using a non-reactive force field (Sorescu et al., 2000; Agrawal et al., 2003), including a prediction of the pressure dependence of the melting point, $T_m = T_m(P)$ (Siavosh-Haghighi & Thompson, 2011; see Fig. 11). Using that same force field Thompson and coworkers have studied the shock strength dependence for (100)-oriented crystals (Siavosh-Haghighi et al., 2009; Dawes et al. 2009). They found that considerable disordering occurs for shock strengths of 2.0 km·s^{-1} and greater. By projecting the instantaneous kinetic energy of individual molecules in the system onto the normal mode eigenvectors for a single molecule in the explicit crystal field they characterized the detailed energy transfer between the shock and molecular translational, rotational, and vibrational modes of the molecule. The results showed that, among the vibrational modes, shock excitation first excites the low-frequency modes; subsequent excitation of higher frequency vibrations occurs on longer time scales, with an approximately monotonic dependence between the frequency of a given mode and the time required for it to reach a steady-fluctuating energy in the shocked state. Further, the detailed energy transfer pathways differ for molecules that are impacted "methyl end first" versus "nitro end first" in the (100) shock orientation. (This latter point is interesting in light of the observation by Nomura et al. (2007a) for the case of reactive ReaxFF (van Duin et al., 2001; Strachan et al., 2005) shocks propagating along [100] in RDX that molecules belonging to the two distinct orientations in the crystal respond differently to the shock; one group of molecules undergoes chemical reaction while the other exhibits flattening and rotation without chemistry.)

He et al. (2011) studied shocks in oriented nitromethane crystals impacted at 2.0 km·s^{-1} using MD with the same force field as Dawes et al. (2009). They observed significant differences in the responses to shocking along the [100], [010], and [001] directions. Jaramillo et al. (2007) studied the shock response of (100)-oriented α-HMX using a non-reactive force field model (Smith & Bharadwaj, 1999; Bedrov et al., 2002) for impact strengths between 0.5 and 2.0 km·s^{-1}. They observed a clear transition between elastic, elastic-plastic, and overdriven behavior in the crystals. Their results show that at lower pressures plasticity is mediated by

the nucleation and spread of crystallographic dislocations, whereas at higher pressures there is a transition from dislocations to the formation of nanoscale shear bands in the material. They noted that regions of material associated with these defects had larger local temperatures. Eason and Sewell (2011) have used a non-reactive force field (Borodin et al., 2008) to study the shock response of (100)- and (001)-oriented PETN. These orientations were found to be insensitive and sensitive, respectively, to shock initiation in the experiments by Dick and coworkers (Dick, 1984; Dick et al., 1991, 1997). For 1.0 $km \cdot s^{-1}$ shocks, Eason and Sewell (2011) observed the formation of defects in (110) planes for (100)-oriented shocks, but only elastic compression for (001)-oriented shocks; see Fig. 12.

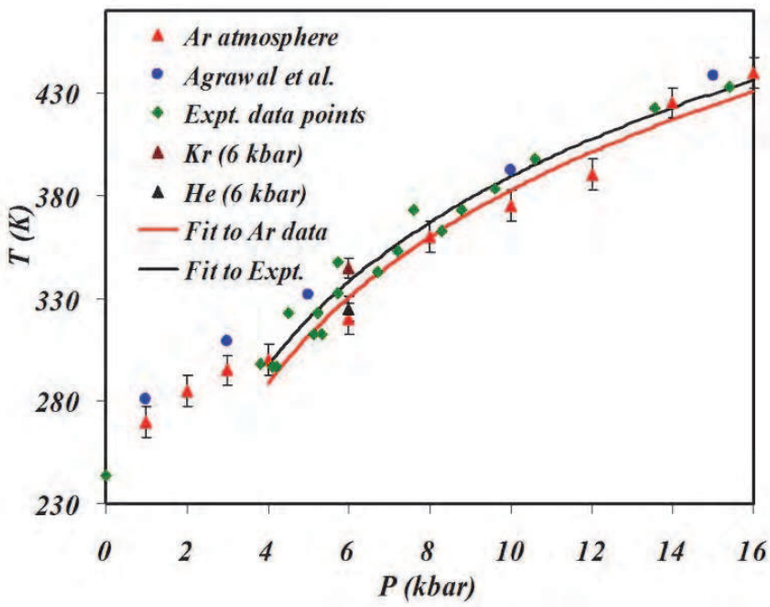

Fig. 11. Computed and experimental melting curves for nitromethane. The MD simulation results were obtained using the SRT force field (Sorescu et al., 2003). See Siavosh-Haghighi & Thompson (2011) and references therein.

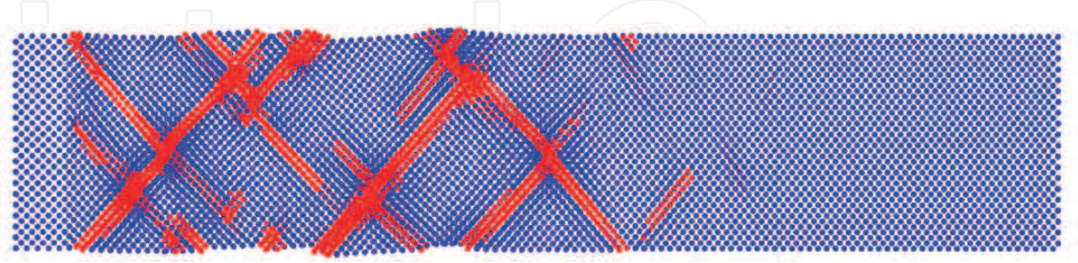

Fig. 12. Snapshot from a MD simulation of a shock wave propagating along [100] in PETN crystal. Only molecular centers of mass are shown. At the left end of the system is a rigid piston; the shock wave propagates from left to right. The snapshot corresponds to the instant of maximum compression (that is, the time when the shock front reaches the right-hand end of the sample). Blue corresponds to the piston, unshocked material, or elastically shock-compressed material. Red corresponds to molecules that have undergone locally inelastic compression.

Zybin and coworkers (Budzien et al. 2009; Zybin et al., 2010) studied the reactive dynamics of PETN using the ReaxFF force field. Budzien et al. studied the onset of chemistry for shocks propagating along [100] with impact velocities of 3 or 4 km·s^{-1}. Zybin et al. (2010) studied the anisotropic initiation sensitivity of PETN in conjunction with a compress-and-shear model. By imposing rapid compression followed by rapid shear, with specific combinations of those two deformation types chosen to emulate the possible interactions between oriented shocks and probable slip systems, they were able to correlate the buildup of stresses, local temperatures, and onset of chemistry with the experimentally observed initiation anisotropy.

Atomic-level simulations of shock waves interacting with pre-existing defects or interfaces have been performed. Various models ranging in complexity from highly schematic (2AB → A_2 + B_2 + ΔH) to relatively realistic (RDX → small molecule products) have been used. Shi and Brenner (2008), using a reactive force field model for the schematic energetic material nitrogen cubane (overall stoichiometry $N_8(s) \rightarrow 4N_2(g)$), have studied the effects of faceted interfaces on energy localization and detonation initiation. These simulations are of particular interest because of discussions of whether, or to what extent, the relative shock insensitivity of certain RDX formulations can be attributed to smoothed crystal edges obtained by treatment by surfactants or mechanical milling. Shi and Brenner identified shock focusing and local compression of the facets as two mechanisms for hotspot formation; which one dominates in a given situation depends on the shock impedance mismatch between the binder and energetic crystal. Using a version of the ReaxFF reactive force field (van Duin, 2001; Strachan, 2005), Nomura et al. (2007b) studied the collapse of single 8-nm diameter cylindrical voids in RDX crystal for the case of shock propagation along the [100] direction, with piston impact velocities of 1 and 3 km·s^{-1} (shock velocities of ~3 and ~9 km·s^{-1}, respectively). They observed the formation of nanojets during void collapse, which led to energy focusing when the jet impinged on the downstream wall of the void. For the weaker shock the local heating from jet impact on the downstream wall remained largely localized near the collapsed jet/wall interface stagnation zone, whereas for the stronger shock a conical region of material extending into the downstream wall underwent vibrational heating. For the stronger shock the dominant reaction during void closure was N-N bond cleavage; smaller reaction products (N_2, H_2O, HONO) were rapidly generated once the nanojet reached the downstream wall. Cawkwell and Sewell (2011) have performed preliminary studies of void collapse in various oriented single crystals of RDX. Figure 13 contains a snapshot, taken when the shock wave reached the far end of the simulation cell, of the molecular centers of mass of an RDX crystal subsequent to the passage of a shock wave with piston impact speed 0.5 km·s^{-1} over a 20 nm cylindrical void in a (210) shock. Molecules initially on the surface of the cylindrical void are colored blue; all others are colored red. The results indicate considerable structural complexity in the shock response, including regions of intense plastic deformation, stacking faults, and a stress-induced phase transition. Note also the large asymmetry of the void collapse process; for the crystal orientation and impact speed chosen, lateral jets form from the top and bottom of the void and collide near the geometric center of the original void. Using a reactive force field for the model reactive diatomic material 2AB → A_2 + B_2 + ΔH, Herring *et al.* (Herring *et al.*, 2010) performed a detailed study, in 2-D, of the effects of void size and geometrical arrangement on thresholds for initiation. They considered a number of geometric arrangements of circular voids including single voids, voids on square and triangular lattices, and randomly arranged voids. Although the AB system is a highly

idealized model, it captures many features of reactive waves in real materials (Heim, 2007, 2008a, 2008b).

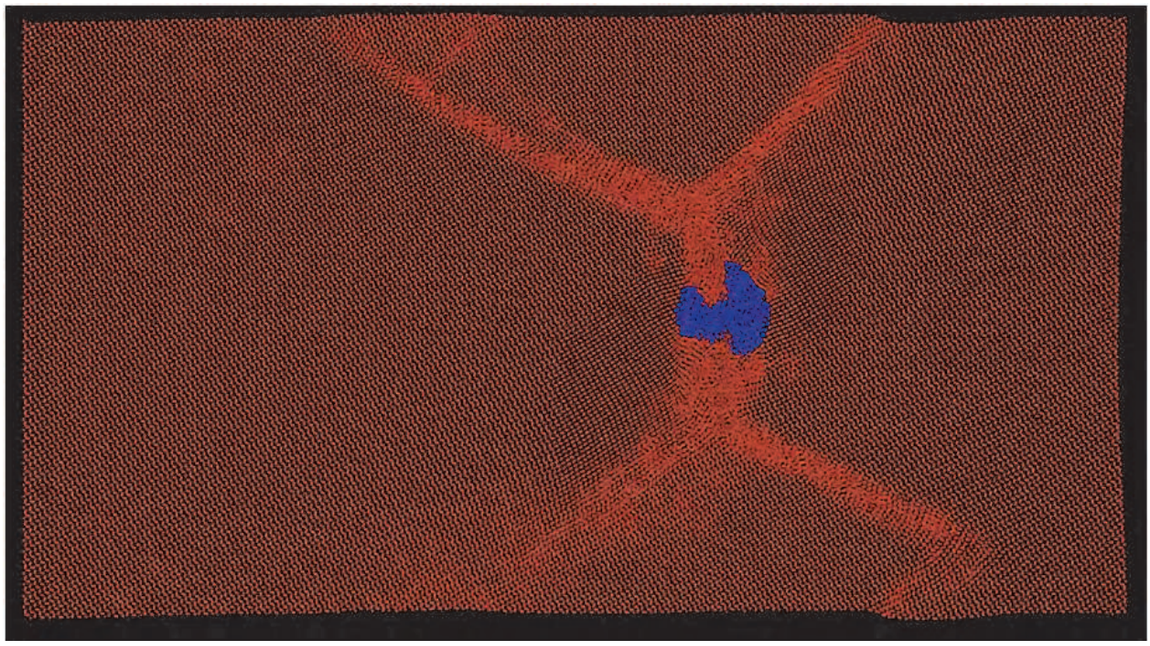

Fig. 13. Snapshot from a MD simulation of void collapse in (210)-oriented RDX. Only molecular centers of mass are shown. (Cawkwell & Sewell, 2011.)

As illustrated by the preceding discussion, MD simulations of energetic materials constituent materials and structures can be used in a variety of ways with objectives that range from near-quantitative predictions of spectroscopic or thermo-mechanical properties needed directly within existing constitutive or reactive burn models but currently unavailable, sparse, or unreliable with present-day experimental methods; to ones designed to reveal or refine existing understanding of fundamental dynamical processes associated with material dynamics (inelastic deformation, stress-induced phase transitions); to more qualitative ones designed to answer basic questions about, for example, material response in the presence of seeded defects and how material response changes with variations in the geometric features of those defects or how the morphology of a heterogeneous system affects the shock-induced localization of energy.

5. Conclusions

An important motivation for the simulation of deformation processes in energetic materials is the desire to avoid accidental ignition of explosives under the influence of a mechanical load. This requires the understanding of material behavior at macro-, meso- and molecular scales.

Experimental methods to determine the sensitivity of energetic materials to an external stimulus can be directly interpreted in terms of test severity in order to rank explosives. Simulation at the macroscale facilitates interpretation of experimental results; for example, by exceeding certain threshold values the ignition of a specific explosive composition is anticipated. Presented thresholds are related to 1) shear rate, 2) a pressure-, shear-rate- and

load-duration-dependent parameter, and 3) a parameter incorporating time-varying pressure and shear-rate loading. The latter two approaches are based on a micro-structural model. Unfortunately, results are applied only to PBX9501 or similar HMX-containing explosive compositions. Starting from the same micro-structural model however, one may arrive at a threshold parameter for PBXs containing energetic crystals other than HMX.

Simulations of PBXs including features from the mesoscale can be categorized as follows. First, one can use continuum models with particle-specific features that are fitted to experimental data and use those continuum models as input for simulations at the macroscale. Secondly, one can determine the collective mechanical behavior by simulation of a representative volume element with the mechanical properties of all individual constituents. And thirdly, one can simulate the mechanical behavior in deformation processes directly at the mesoscale, and interpret the results in terms of probabilistic distribution functions of wave field variables.

Atomic-level simulations of energetic materials can be used to predict physical properties such as equations of state, transport coefficients, and spectroscopic features, and to study fundamental processes such as energy transfer, inelastic deformation, phase transitions, and reaction chemistry. These are among the properties needed for the development and parameterization of improved mesoscale models. Depending on the accuracy of the force field used, these predictions can be expected to be semi-quantitative or to reveal general features of materials behavior in complicated polyatomic materials. Studies of the effects of defects, voids, or material interfaces on the physical properties and dynamic response can be studied in detail; although the results must be interpreted with caution if the goal is to link directly to the mesoscale, due to the disparity between defect sizes or number densities that can be simulated using MD and those that occur in real materials.

6. Acknowledgments

The authors acknowledge support from the U. S. Defense Threat Reduction Agency. R.H.B.B. and A.E.D.M.H. acknowledge support from The Netherlands Ministry of Defence. T.D.S. acknowledges support from the U. S. Office of Naval Research and the Los Alamos National Laboratory LDRD program. T.D.S and D.L.T. acknowledge support from a DOD MURI grant managed by the U. S. Army Research Office.

7. References

Agrawal, P.M., Rice, B.M., Zheng, L., & Thompson, D.L. (2006). Molecular dynamics simulations of hexahydro-1,3,5-trinitro-1,3,5-*s*-triazine (RDX) using a combined Sorescu-Rice-Thompson AMBER force field. *Journal of Physical Chemistry B* 110, 26185.

Agrawal, P.M., Rice, B.M. & Thompson, D.L. (2003). Molecular dynamics studies of the melting of nitromethane. *Journal of Chemical Physics* 119, 9617.

Armstrong, R. W. (2009). Dislocation mechanics aspects of energetic material composites. In: *Reviews on Advanced Materials Science 19*, Ovid'ko, I.A., (Ed), pp. 14-34.

Autodyn, http://www.ansys.com/Products/Simulation+Technology/Explicit+Dynamics/ANSYS+AUTODYN.

Baer, M.R. & Trott, W.M. (2002). Theoretical and experimental mesoscale studies of impact-loaded granular explosive and simulant materials. *Proceedings of 12th International Detonation Symposium*, San Diego, USA, August 2002.

Baer, M.R. (2002). Modeling heterogeneous energetic materials at the mesoscale. *Thermochimica Acta* 384, 351.

Bailly, P., Delvare, F., Vial, J., Hanus, J. L., Biessy, M. & Picart, D. (2011). Dynamic behavior of an aggregate material at simultaneous high pressure and strain rate: SPHB triaxial tests. *International Journal of Impact Engineering*, 38, (2011), pp. 73-84.

Bardenhagen, S.G., Brydon, A.D., Williams, T.O. & Collet, C. (2006). Coupling grain scale and bulk mechanical response for PBXs using numerical simulations of real microstructures. *AIP Conference Proceedings*, 845 (2006), pp. 479-482.

Barton, N.R., Winter, N.W. & Reaugh, J. E. (2009). Defect evolution and pore collapse in crystalline energetic materials. *Modelling and Simulation in Materials Science and Engineering*, 17, 035003.

Bedrov, D., Smith, G.D. & Sewell, T.D. (2000). Temperature-dependent shear viscosity coefficient of octahydro-1,3,5,7-tetranitro-1,3,5,7-tetrazocine (HMX): A molecular dynamics simulation study. *Journal of Chemical Physics* 112, 7203.

Bedrov, D., Ayyagari, C., Smith, G.D., Sewell, T.D., Menikoff, R. & Zaug, J.M. (2001). Molecular dynamics simulations of hmx crystal polymorphs using a flexible molecule force field, *Journal of Computer-Aided Materials Design* 8, 77.

Bedrov, D., Smith, G.D. & Sewell, T.D. (2003). Thermodynamic and mechanical properties from atomistic simulations, in *Energetic Materials, Volume 12: Part 1. Decomposition, Crystal, and Molecular Properties (Theoretical and Computational Chemistry)*, Murray, J.S. and Politzer, P. Eds. (Elsevier, Amsterdam).

Bedrov, D., Borodin, O., Smith, G.D., Sewell, T.D., Dattelbaum, D.M. & Stevens, L.L. (2009). A molecular dynamics simulation study of crystalline 1,3,5-triamino-2,4,6,trinitrobenzene as a function of pressure and temperature. *Journal of Chemical Physics* 131, 224703.

Bennett, J.G., Haberman, K.S., Johnson, J.N., Asay, B.W. & Henson, B.F. (1998). A constitutive model for the non-shock ignition and mechanical response of high explosives. *J. Mech. Phys. Solids*, 46, (1998), pp. 2302-2322.

Birnbaum, N.K., Cowler, M.S., Itoh, M., Katayama, M. & Obata, H. (1987). AUTODYN – an interactive nonlinear dynamic analysis program for microcomputers through supercomputers. *Proceedings of 9th Int. Conf. on Structural Mechanics in Reactor Technology*, Lausanne, Switzerland, 1987.

Bock, N., Challacombe, M., Gan, C.-K., Henkelman, G., Nemeth, K., Niklasson, A.M.N., Odell, A., Schwegler, E., Tymczak, C.J. & Weber, V. (2011). FreeON. Los Alamos National Laboratory (LA-CC 01-2, LA-CC-04-086) http://freeon.org.

Borodin, O., Smith, G.D., Sewell, T.D., and Bedrov, D. (2008). Polarizable and nonpolarizable force fields for alkyl nitrates. *Journal of Physical Chemistry* B 112, 734.

Bouma, R.H.B., Courtois, C., Verbeek, H.J. & Scholtes, J.H.G. (1999). Influence of mechanical damage on the shock sensitivity of plastic bonded explosives. *Proceedings of Insensitive Munitions & Energetic Materials Technology Symposium*, Tampa, USA, November 1999.

Bouma, R.H.B., Verbeek, H.J. & van Wees, R.M.M. (2003). Design of barriers for the prevention of sympathetic detonation in out-of-area munition storage. *Proceedings of 30th International Pyrotechnics Seminar*, Saint Malo, France, June 2003.

Bouma, R.H.B. & Meuken, B. (2004). Explosive and mechanical deformation of PBXN-109. *Proceedings of workshop on shear stress evaluation and contribution to the ignition of PBX*, Institut für Chemische Technologie, Pfinztal, Germany, June 2004.

Bouma, R.H.B., Meuken, B. & Verbeek, H.J. (2007). Shear initiation of Al/MoO3-based reactive materials. *Propellants, Explosives, Pyrotechnics*, 32, (2007), pp. 447-453.

Bowden, F.P. & Yoffe, Y.D. (1952). *Initiation and growth of explosion in liquids and solids*, Cambridge University Press, ISBN 0 521 31233 7, Cambridge, United Kingdom.

Browning, R.V. (1995). Microstructural model of mechanical initiation of energetic materials. *Proceedings of APS Conference on Shock Compression of Condensed Matter,* Seattle, USA.

Browning, R.V. & Scammon, R.J. (2001). Microstructural modal of ignition for time varying loading conditions, *Proceedings of APS Conference on Shock Compression of Condensed Matter,* CP620, 987-990.

Browning, R.V. & Scammon, R.J. (2002). Influence of mechanical properties on non-shock ignition. *Proceedings of 12th Int. Detonation Symposium*, San Diego, USA, August 2002.

Budzien, J., Thompson, A.P. & Zybin, S.V. (2009). Reactive molecular dynamics simulations of shock through a single crystal of pentaerythritol tetranitrate. *Journal of Physical Chemistry B* 113, 13142.

Cawkwell, M.J., Sewell, T.D., Zheng. L & Thompson, D.L. (2008). Shock-induced shear bands in an energetic molecular crystal: Application of shock-front absorbing boundary conditions to molecular dynamics simulations, *Physical Review B* 78, 014107.

Cawkwell, M.J., Ramos, K.J., Hooks, D.E. & Sewell, T.D. (2010). Homogeneous dislocation nucleation in cyclotrimethylene trinitramine under shock loading. *Journal of Applied Physics* 107, 063512.

Cawkwell, M.J. and Sewell, T.D. (2011). Unpublished results.

Chen, Y.-C., Nomura, K.-i., Kalia, R.K., Nakano, A. & Vashishta, P. (2008). Molecular dynamics nanoindentation simulation of an energetic material. *Applied Physics Letters* 93, 171908.

Chidester, S.K., Tarver, C.M. & Garza, R. (1998). Low amplitude impact testing and analysis of pristine and aged solid high explosives. *Proceedings of 11th Int. Detonation Symposium*, Snowmass, USA.

Coe, J.D., Sewell, T.D. & Shaw, M.S. (2009). Optimal sampling efficiency in Monte Carlo simulation with an approximate potential. *Journal of Chemical Physics* 130, 164104.

Coe, J.D., Sewell, T.D. & Shaw, M.S. (2009). Nested Markov chain Monte Carlo sampling of a density functional theory potential: Equilibrium thermodynamics of dense fluid nitrogen. *Journal of Chemical Physics* 131, 074105.

Coffey, C.S. (1995). Impact testing of explosives and propellants. *Propellants, Explosives, Pyrotechnics*, 20, (1995), pp. 105-115.

Coffey, C.S. & Sharma, J. (1999). Plastic deformation, energy dissipation, and initiation of crystalline explosives. *Physical Review B – Condensed Matter and Materials Physics*, 60, (1999), pp. 9365-9371.

Conley, P.A. & Benson, D.J. (1999). An estimate of the linear strain rate dependence of octahydro-1,3,5,7-tetranitro-1,3,5,7-tetrazocine. *Journal of Applied Physics*, 939. (199), pp. 6717-6728.

Dawes, R., Siavosh-Haghighi, A., Sewell, T.D. & Thompson, D.L. (2009). Shock-induced melting of (100)-oriented Nitromethane: Energy partitioning and vibrational mode heating. *Journal of Chemical Physics* 131, 224513.

De, S. & Macri, M. (2006). Modeling the bulk mechanical response of heterogeneous explosives based on microstructural information. *Proceedings of 13th Int. Detonation Symposium* 373., Norfolk, USA.

Desbiens, N., Bourasseau, E. & Maillet, J.-B. (2007). Potential optimization for the calculation of shocked liquid nitromethane properties, *Molecular Simulation* 33, 1061.

Desbiens, N., Bourasseau, E., Maillet, J.-B. & Soulard, L. (2009). Molecular based equation of state for shocked liquid nitromethane. *Journal of Hazardous Materials* 166, 1120.

Dick, J.J. (1984). Effect of crystal orientation on shock initiation sensitivity of pentaerythritol tetranitrate explosive. *Applied Physics Letters* 44, 859.

Dick, J.J., Mulford, R.N., Spencer, W.J., Pettit, D.R., Garcia, E. & Shaw, D.C., (1991). Shock response of pentaerythritol tetranitrate single crystals. *Journal of Applied Physics* 70, 3572.

Dick, J.J. (1997). Anomalous shock initiation of detonation in pentaerythritol tetranitrate crystals. *Journal of Applied Physics* 81 601.

Dienes, J.K. (1985). A statistical theory of fragmentation processes, *Mechanics of Materials*, Vol 4, 325-335.

Dienes, J.K., Zuo, Q.H. & Kersher, J.D. (2006). Impact initiation of explosives and propellants via statistical crack mechanics. *Journal of the Mechanics and Physics of Solids* 54, 1237.

Doherty, R.M. & Watt, D.S. (2008). Relationship between RDX properties and sensitivity. *Propellants, Explosives, Pyrotechnics*, 33, (2008), pp. 4-13.

DYNA3D (2005). User Manual, Available from https://www-eng.llnl.gov/pdfs/mdg_dyna3d.pdf

Eason, R.M. and Sewell, T.D. (2011). Unpublished results.

Frenkel, D. & Smit. B. (2002) *Understanding Molecular Simulation*, 2nd Ed. (Academic Press, San Diego.)

Gee, R.H., Wu, C. & Maiti, A. (2006). Coarse-grained model for a molecular crystal. *Applied Physics Letters* 89, 021919.

Goddard, W.A., Meiron, D.I., Ortiz, M., Shepherd, J.E. & Pool, J. (1998). *Technical Report 032, Center for Simulation of Dynamic Response in Materials*, California Institute of Technology. http://www.cacr.caltech.edu/ASAP/publications/cit-asci-tr/cit-asci-tr032.pdf.

Goldman, N., Reed, E.J. & Fried, L.E. (2009). Quantum mechanical corrections to simulated shock Hugoniot temperatures. *Journal of Chemical Physics* 131, 204103.

Gruau, C., Picart, D., Belmas, R., Bouton, E., Delmaire-Sizes, F., Sabatier, J. & Trumel, H. (2009). Ignition of a confined high explosive under low velocity impact. *International Journal of Impact Engineering*, 36, (2009), pp. 537-550.

Hager, K., Tancreto, J. & Swisdak, M. (2000). High Performance Magazine non-progation wall design criteria. *Proceedings of 29th DDESB Seminar*, New Orleans, USA, July 2000.

Han, S.-p., van Duin, A.C.T., Goddard, W.A. III & Strachan, A. (2011) Thermal decomposition of condensed-phase nitromethane from molecular dynamics from ReaxFF reactive dynamics. *Journal of Physical Chemistry B* 115, 6534.

Handley, C.A. (2011). Numerical modeling of two HMX-based plastic-bonded explosives at the mesoscale. Ph. D. thesis, St. Andrews University. Available from http://research-repository.st-andrews.ac.uk

Haussühl, S. (2001). Elastic and thermoelastic properties of selected organic crystals: acenaphthene, trans-azobenzene, benzophenone, tolane, trans-stilbene, dibenzyl, diphenyl sulfone, 2,20-biphenol, urea, melamine, hexogen, succinimide, pentaerythritol, urotropine, malonic acid, dimethyl malonic acid, maleic acid, hippuric acid, aluminium acetylacetonate, iron acetylacetonate, and tetraphenyl silicon. *Z. Kristallogr*. 216, 339.

Haycraft, J.J., Stevens, L.L., & Eckhardt, C.J. (2006). The elastic constants and related properties of the energetic material cyclotrimethylene trinitramine (RDX) determined by Brillouin scattering, *Journal of Chemical Physics*, 124, 024712.

He, L. Sewell, T.D. & Thompson, D.L. (2011). Molecular dynamics simulations of shock waves in oriented nitromethane single crystals. *Journal of Chemical Physics* 134, 124506.

Heim, A.J., Grønbech-Jensen, N., Germann, T.C., Holian, B.L., Kober, E.M. & Lomdahl, P.S. (2007). Influence of interatomic bonding potentials on detonation properties. *Physical Review E* 76, 026318.

Heim, A.J., Grønbech-Jensen, N., Kober, E.M., Erpenbeck, J.J. & Germann, T.C. (2008a). Interaction potential for atomic simulations of conventional high explosives. *Physical Review E* 78, 046709.

Heim, A.J., Grønbech-Jensen, N. Kober, E.M. & Germann, T.C. (2008b). Molecular dynamics simulations of detonation instability. *Physical Review E* 78, 046710.

Hooks, D.E., Ramos, K.J. & Martinez, A.R. (2006). Elastic-plastic shock wave profiles in oriented single crystals of cyclotrimethylene trinitramine (RDX) at 2.25 GPa. *Journal of Applied Physics* 100, 024908.

Hoover, W.G. (1985). Canonical dynamics: Equilibrium phase-space distributions. *Physical Review A* 31, 1695.

Hsu, P.C., Hust, G., Howard, M. & Maienschein, J.L. (2010). The ODTX system for thermal ignition and thermal safety study of energetic materials, *Proceedings of the 14th Int. Detonation Symposium*, Coeur D'Alene, USA

Izvekov, S., Chung, P.W. & Rice, B.M. (2010). The multiscale coarse-graining method: Assessing its accuracy and introducing density dependent coarse-grain potentials. *Journal of Chemical Physics* 133, 064109.

Jaidann, M., Lussier, L.-S., Bouamoul, A., Abou-Rachid, H. & Brisson, J. (2009). Effects of interface interactions on mechanical properties in RDX-based PBXs HTPB-DOA: Molecular dynamics simulations. In *Lecture Notes in Computer Science* 5545 (Proceedings of the ICCS, 2009, Part II). Allen, G. et al. (Eds.) (Springer-Verlag, Berlin) 131.

Jaramillo, E., Sewell, T.D. & Strachan, A. (2007). Atomic-level view of inelastic deformation in a shock loaded molecular crystal. *Physical Review B* 76, 064112.

Jaramillo-Botero, A., Nielsen, R., Abrol, R., Su, J. Pascal, T., Mueller, J. & Goddard, W.A. III (2011). First-principles-based multiscale, multiparadigm molecular mechanics and

dynamics methods for describing complex chemical processes. *Top. Curr. Chem.* DOI: 10.1007/128_2010_114 (Springer-Verlag, Heidelberg).

Koch, W. & Holthausen, M.C. (2001). *A Chemist's Guide to Density Functional Theory*, 2nd Ed. (Wiley-VCH, Wenheim).

Kolb, J.R. & Rizzo, H.F. (1979). Growth of 1,3,5-triamino-2,4,6-trinitrobenzene (TATB) I. Anisotropic thermal expansion. *Propellants, Explosives, and Pyrotechnics* 4, 10.

Kresse, G. et al. (2011). Vienna *Ab Initio* Simulation Package (VASP), Department of Computational Physics, Universität Wien, Wien, Austria, http://cms.mpi.univie.ac.at/vasp/.

Kuklja, M. & Rashkeev, S.N. (2009). Interplay of decomposition mechanisms at shear-strain interface. *The Journal of Physical Chemistry C* 113, pp. 17-20.

Lee, E.L. & Tarver, C.M., Phenomenological model of shock initiation in heterogeneous explosives. *Physics of Fluids*, Vol. 23 (1980), p. 2362.

Lei, L. & Koslowski, M., (2011). Mesoscale modeling of dislocations in molecular crystals. *Philosophical Magazine* 91, 865.

Lin, P.-H., Khare, R., Weeks, B.L. & Gee, R.H. (2007). Molecular modeling of diffusion on a crystalline pentaerythritol tetranitrate surface. *Applied Physics Letters* 91, 104107.

Liu, A. & Stuart, S.J. (2008). Empirical bond-order potential for hydrocarbons: Adaptive treatment of van der Waals interactions. *Journal of Computational Chemistry* 29, 601.

Lynch, K., Thompson, A. & Strachan, A. (2009) Coarse-grain modeling of spall failure in molecular crystals: Role of intra-molecular degrees of freedom. *Modelling and Simulation in Materials Science and Engineering* 17, 015007.

Maillet, J.-B. & Stoltz, G. (2008). Sampling constraints in average: The example of Hugoniot curves. *Applied Mathematics Research eXpress* 2008, abn004.

Malvar, L.J. (1994). Development of HPM nonpropagation walls: test results and Dyna3D predictions of acceptor response. *Proceedings of 26th DDESB Seminar*, New Orleans, USA, August 1994.

Manaa, M.R., Reed, E.J., Fried, L.E. & Goldman, N. (2009). Nitrogen-rich heterocycles as reactivity retardants in shocked insensitive explosives. *Journal of the American Chemical Society* 131, 5483.

Martyna, G.J., Tuckerman, M.E., Tobias, D.J. & Klein, M.L. (1996). Explicit reversible integration algorithms for extended systems dynamics. *Molecular Physics* 87, 1117.

Menikoff, R. & Sewell, T.D. (2002). Constituent properties of HMX needed for mesoscale simulations. *Combustion Theory and Modeling* 6, 103.

Menikoff, R., Dick, J. J. & Hooks, D. E.(2005). Analysis of wave profiles for single-crystal cyclotetramethylene tetranitramine. *Journal of Applied Physics* 97, 023529.

Menikoff, R. (2008). Comparison of constitutive models for plastic-bonded explosives. *Combustion Theory and Modeling* 12, 73.

Menikoff, R. (2011). Hot spot formation from shock reflections. *Shock Waves* 21, 141.

Metropolis, N. Rosenbluth, A.W., Rosenbluth, M.N., Teller, A.H. & Teller, E. (1953). Equation of state calculations by fast computing machines. *Journal of Chemical Physics* 21, 1087.

Meuken, B., Martinez Pacheco, M., Verbeek, H.J., Bouma, R.H.B. & Katgerman, L. (2006). Shear initiated reactions in energetic and reactive materials. *Mater. Res. Soc. Symp. Proc. Vol. 896*, (2006) 0896-H06-06, pp. 1-6.

Millar, D.I.A., Oswald, I.D.H., Barry, C., Francis, D.J., Marshall, W.G., Pulham, C.R. & Cumming, A.S. (2010). Pressure-cooking of explosives – the crystal structure of ε-RDX as determined by X-ray and neutron diffraction. *Chemical Communication*s 46, 5662.

Molt, R.W. Jr., Watson, T. Jr., Lotrich, V.F. & Bartlett, R.J. (2011). RDX geometries, excited states, and revised energy ordering of conformers via MP2 and CCSD(T) methodologies: Insights into decomposition mechanism. *Journal of Physical Chemistry A* 115, 884.

Munday, L. B., Chung., P. W., Rice, B. M., and Solares, S. D. (2011). Simulations of high-pressure phases in RDX. *Journal of Physical Chemistry B* 115, 4378.

Namkung, J. & Coffey, C.S. (2001). Plastic deformation rate and initiation of crystalline explosives. *Proceedings of Shock Compression of Condensed Matter,* Furnish, M.D., Thadhani, N.N. & Horie, Y. (Eds), CP620, (2001), pp. 1003-1006.

Nomura, K.-i., Kalia, R.K., Nakano, A. & Vashishta, P. (2007a). Dynamic transition in the structure of an energetic crystal during chemical reactions at shock front prior to detonation. *Physical Review Letters* 99, 148303.

Nomura, K.-i., Kalia, R.K., Nakano, A. & Vashishta, P. (2007b). Reactive nanojets: Nanostructure-enhanced chemical reactions in a defected energetic crystal. *Applied Physics Letters*, 91, 183109.

Nosé, S. (1984). A unified formulation of the constant temperature molecular dynamics methods. *Journal of Chemical Physics* 81, 511.

Parrinello, M. & Rahman, A. (1981). Polymorphic transitions in single crystals: A new molecular dynamics method. *Journal of Applied Physics* 52, 7182.

Ramos, K.J., Hooks, D.E. & Bahr, D.F. (2009). Direct observation of plasticity and quantitative hardness measurements in single crystal cyclotrimethylene trinitramine by nanoindentation. *Philosophical Magazine* 89, 2381.

Ramos, K.J., Hooks, D.E., Sewell, T.D. & Cawkwell, M.J. (2010). Anomalous hardening under shock compression in (021)-oriented cyclotrimethylene trinitramine single crystals. *Journal of Applied Physics* 108, 066105.

Ravelo, R., Holian, B.L., Germann, T.C. & Lomdahl, P.S. (2004). Constant-stress Hugoniostat method for following the dynamical evolution of shocked matter. *Physical Review B* 70, 014103.

Reaugh, J.E. (2002). Grain-scale dynamics in explosives, Lawrence Livermore National Laboratory Unclassified Report UCRL-ID-150388.

Reed, E.J., Fried, L.E. & Joannopoulos, J.D. (2003). A method for tractable dynamical studies of single and double shock compression. *Physical Review Letters* 90, 235503.

Rice, B.M. & Sewell, T.D. (2008). Molecular dynamics simulations of energetic materials at thermodynamic equilibrium, in *Energetic Materials at Static High Pressures*, Piermarini G. and Peiris, S.M., Eds. (Springer-Verlag, Heilderberg).

Sandusky, H.W., Paul Chamber, G. & Carlson, V.J. (1998). Setback simulation of fielded and candidate explosive fill for 5″/54 guns. *Proceedings of 1998 JANNAF Propulsion Systems Hazards Subcommittee Meeting*, CPIA Publ. 681, Vol. II, p. 137-145.

Scammon, R.J., Browning, R.V., Middleditch, J., Dienes, J.K., Haberman, K.S. & Bennett, J.G. (1998). Low amplitude insult project: structural analysis and prediction of low order reaction. *Proceedings of 11th Int. Detonation Symposium*, Snowmass, USA, August 1998.

Scholtes, J.H.G., Bouma, R.H.B., Weterings, F.P., & van der Steen, A.C. (2002). Thermal and mechanical damage of PBXs. *Proceedings of 12th International Detonation Symposium*, San Diego, USA, August 2002.

Schwarz, R.B., Hooks, D.E., Dick, J.J., Archuleta, J.I., and Martinez, A.R. (2005). Resonant ultrasound spectroscopy measurement of the elastic constants of cyclotrimethylene trinitramine. *Journal of Applied Physics* 98, 056106.

Sewell, T. D., and Bennett, C. M. (2000). Monte Carlo calculations of the elastic moduli and pressure-volume-temperature equation of state for hexahydro-1,3,5-trinitro-1,3,5-triazine. *Journal of Applied Physics* 88, 88.

Sewell, T.D. (2008). Atomistic-based mesoscopic constitutive models for high explosive constituent materials. *Final report for project 49449-EG*, (2008).

Sewell, T.D., Menikoff, R., Bedrov, D. & Smith, G.D. (2003). A molecular dynamics simulation study of elastic properties of HMX. *Journal of Chemical Physics* 119, 7417.

Shane Stafford, D. & Jackson, T.L. (2010). Using level sets for creating virtual random packs of non-spherical convex shapes. *Journal of Computational Physics* 229, (2010), 3295-3315.

Shi, Y. & Brenner, D.W. (2008). Molecular simulation of the influence of interface faceting on the shock sensitivity of a model plastic bonded explosive, *Journal of Physical Chemistry B* 112, 14898.

Siavosh-Haghighi, A., & Thompson, D.L. (2006). Molecular dynamics simulations of surface-initiated melting of nitromethane. *Journal of Chemical Physics* 125, 184711.

Siavosh-Haghighi, A., Dawes, R., Sewell, T.D. & Thompson, D.L. (2009). Shock-induced melting of (100)-oriented nitromethane: Structural relaxation. *Journal of Chemical Physics* 131, 064503.

Siavosh-Haghighi, A., Sewell, T.D., and Thompson, D.L. (2010). Molecular dynamics study of the crystallization of nitromethane from the melt. *Journal of Chemical Physics* 133, 194501.

Siavosh-Haghighi, A. and Thompson, D.L. (2011). Unpublished results.

Siviour, C.R., Williamson, D.M., Grantham, S.G., Palmer, S.J.P., Proud, W.G. & Field, J.E. (2004), Split Hopkinson bar measurements of PBXs, In: *Shock Compression of Condensed Matter*, Furnish, M.D., Gupta, Y.M. & Forbes, J.W. (eds.), CP706, American Institute of Physics.

Smith, G. D. & Bharadwaj, R.K. (1999). Quantum chemistry based force field for simulations of HMX. *Journal of Physical Chemistry B* 103, 3570.

Sorescu, D.C., Rice, B.M. & Thompson, D.L. (2000). Theoretical studies of solid nitromethane. *Journal of Physical Chemistry B* 104, 8406.

Stevens, L.L., & Eckhardt, C. J. (2005). The elastic constants and related properties of β-HMX determined by Brillouin scattering, *Journal of Chemical Physics* 122, 174701.

Strachan, A. & Holian, B.L. (2005). Energy exchange between mesoparticles and their internal degrees of freedom. *Physical Review Letters* 94, 014301.

Strachan, A., Kober, E.M., van Duin, A.C.T., Oxgaard, J. & Goddard III, W.A. (2005). Thermal decomposition of RDX from reactive molecular dynamics. *The Journal of Chemical Physics*, 122, 054502.

Stuart, S.J., Tutein, A.B., & Harrison, J.A. (2000). A reactive potential for hydrocarbons with intermolecular interactions. *Journal of Chemical Physics* 112, 6472.

Sun, B., Winey, J.M., Hemmi, N., Dreger, Z.A., Zimmerman, K.A., Gupta, Y.M., Torchinsky, D.H., & Nelson, K.A. (2008). Second-order elastic constants of pentaerythritol tetranitrate and cyclotrimethylene trinitramine using impulsive stimulated thermal scattering, *Journal of Applied Physics* 104, 073517.

Sun, B., Winey, J. M, Gupta, Y. M., & Hooks, D. E. (2009). Determination of second-order elastic constants of cyclotetramethylene tetranitramine (β-HMX) using impulsive stimulated thermal scattering. *Journal of Applied Physics* 106, 053505.

Swantek, A.B. & Austin, J.M. (2010). Collapse of void arrays under stress wave loading. *Journal of Fluid Mechanics* 649, 399.

Tancreto, J., Swisdak, M. & Malvar, J. (1994). High Performance Magazine acceptor threshold criteria. *Proceedings of 26th DDESB Seminar*, Miami, USA, August 1994.

Thompson, D., Sewell, T., Bouma, R.H.B. & van der Heijden, A.E.D.M. (2010). Investigation of fundamental processes and crystal-level defect structures in metal-loaded high-explosive materials under dynamic thermo-mechanical loads and their relationships to impact survivability of munitions. Project HDTRA1-10-1-0078.

Tuckerman, M.E. (2010). *Statistical Mechanics: Theory and Molecular Simulation* (Oxford University Press, U.S.A.)

Tuckerman, M.E. & Klein, M.L. (1998). Ab initio molecular dynamics study of solid nitromethane. *Chemical Physics Letters* 283, 147.

UN (2008). *Recommendations on the transport of dangerous goods, Manual of tests and criteria*. Available from https://unp.un.org/Details.aspx?pid=17299.

Van Duin, A.C.T., Dasgupta, S., Lorant, F. & Goddard, W. A. III (2001). ReaxFF: A reactive force field for hydrocarbons. *Journal of Physical Chemistry A* 105, 9396.

Van der Heijden, A.E.D.M. & Bouma, R.H.B. (2004). Crystallization and characterization of RDX, HMX and Cl-20. *Crystal Growth and Design*, 4, (2004), 999-1007.

Van der Heijden, A.E.D.M., Bouma, R.H.B. & van der Steen, A.C. (2004). Physicochemical parameters of nitramines determining shock sensitivity. *Propellants, Explosives, Pyrotechnics* 29 (2004) 304-313.

Van der Heijden, A.E.D.M. & Bouma, R.H.B. (2010). Energetic Materials: Crystallization and Characterization, in: *Handbook of Material Science Research*, eds. René, C. & Turcotte, E., 2010, ISBN 978-1-60741-798-9.

Vandersall, K.S., Switzer, L.L. & Garcia, F. (2006). Threshold studies on TNT, Composition B, C-4 and ANFO explosives using the Steven impact test. *Proceedings of 13th Int. Detonation Symposium*, Norfolk, USA, July 2006.

Van Wees, R.M.M., van Dongen, Ph. & Bouma, R.H.B. (2004). The participation of the Netherlands in the UK/AUS defense trial 840. Study of barricades to prevent sympathetic detonation in field storage. *Proceedings of 31th DoD Explosives Safety Seminar*, San Antonio, USA, August 2004.

Wallace, I.G. (1994). Spigot Intrusion. *Proceedings of 26th DoD Explosives Safety Seminar*, Miami, USA.

Winey, J.M. & Gupta, Y.M. (2001). Second-order elastic constants for pentaerythritol tetranitrate single crystals. Journal of Applied Physics 90, 1669.

Winey, J.M. & Gupta, Y.M. (2010). Anisotropic material model and wave propagation simulations for shocked pentaerythritol tetranitrate single crystals. *Journal of Applied Physics* 107, 103505.

Wood, W.W. (1968) in *Physics of Simple Fluids*, edited by Temperley, H.N.V., Rowlinson, J.S., and Rushbrooke G.S. (North-Holland, Amsterdam), Ch. 5, p. 115.

Yan-Qing, W. & Feng-Lei, H. (2009). A micromechanical model for predicting combined damage of particles and interface debonding in PBX explosives. *Mechanics of Materials*, 41, (2009), 27-47.

Zamiri, A.R. & De, S. (2010). Deformation distribution maps of β-HMX molecular crystals. *Journal of Physics D: Applied Physics* 43, 035404.

Zaug, J. M. (1998). Elastic constants of β-HMX and tantalum, equations of state of supercritical fluids and mixtures and thermal transport determinations. *Proceedings of the 11th International Detonation Symposium*, Snowmass, CO, Aug 31-Sept 4, 498.

Zerilli, F.J., Guirguis, R.H. & Coffey, C.S. (2002). A burn model based on heating due to shear flow: proof of principle calculations. *Proceedings of 12th Int. Detonation Symposium*, San Diego, USA, August 2002.

Zerilli, F.J. & Kuklja, M.M. (2007). *Ab initio* equation of state of an organic molecular crystal: 1,1-diamino-2,2-dinitroethylene. *Journal of Physical Chemistry A* 111, 1721.

Zheng, L., Luo, S.-N., & Thompson, D.L. (2006). Molecular dynamics simulations of melting and the glass transition in nitromethane. *Journal of Chemical Physics* 124, 154504.

Zybin, S.V., Goddard III, W.A., Xu, P., van Duin, A.C.T. & Thompson, A.P. (2010). Physical mechanism of anisotropic sensitivity in pentaerythritol tetranitrate from compressive-shear reaction dynamics simulations. *Applied Physics Letters* 96, 081918.

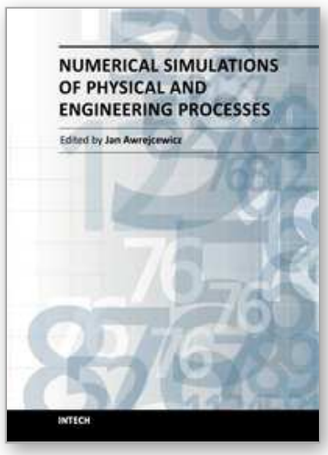

Numerical Simulations of Physical and Engineering Processes

Edited by Prof. Jan Awrejcewicz

ISBN 978-953-307-620-1
Hard cover, 594 pages
Publisher InTech
Published online 26, September, 2011
Published in print edition September, 2011

Numerical Simulations of Physical and Engineering Process is an edited book divided into two parts. Part I devoted to Physical Processes contains 14 chapters, whereas Part II titled Engineering Processes has 13 contributions. The book handles the recent research devoted to numerical simulations of physical and engineering systems. It can be treated as a bridge linking various numerical approaches of two closely inter-related branches of science, i.e. physics and engineering. Since the numerical simulations play a key role in both theoretical and application oriented research, professional reference books are highly needed by pure research scientists, applied mathematicians, engineers as well post-graduate students. In other words, it is expected that the book will serve as an effective tool in training the mentioned groups of researchers and beyond.

How to reference

In order to correctly reference this scholarly work, feel free to copy and paste the following:

R.H.B. Bouma, A.E.D.M. van der Heijden, T.D. Sewell and D.L. Thompson (2011). Simulations of Deformation Processes in Energetic Materials, Numerical Simulations of Physical and Engineering Processes, Prof. Jan Awrejcewicz (Ed.), ISBN: 978-953-307-620-1, InTech, Available from: http://www.intechopen.com/books/numerical-simulations-of-physical-and-engineering-processes/simulations-of-deformation-processes-in-energetic-materials

INTECH
open science | open minds

InTech Europe
University Campus STeP Ri
Slavka Krautzeka 83/A
51000 Rijeka, Croatia
Phone: +385 (51) 770 447
Fax: +385 (51) 686 166
www.intechopen.com

InTech China
Unit 405, Office Block, Hotel Equatorial Shanghai
No.65, Yan An Road (West), Shanghai, 200040, China
中国上海市延安西路65号上海国际贵都大饭店办公楼405单元
Phone: +86-21-62489820
Fax: +86-21-62489821

IntechOpen